Dalton Transactions

ROYAL SOCIETY OF CHEMISTRY

PAPER

View Article Online
View Journal | View Issue

Cite this: *Dalton Trans.*, 2024, **53**, 17547

Effect of ligand substituents on the reactivity pathways of copper(II) complexes towards electrocatalytic water oxidation†

Hemrupa Kuilya,[a] Pranjal Das,[a] Swati Basak,[a] Debajit Sarma,[b] Pradyumna Mazumdar,[a] Diganta Choudhury *[a] and Apurba Kalita *[a]

The electrocatalytic water oxidation activity of three copper(II) complexes [Cu($\mathbf{L_1H}$)(L_1)](ClO_4) (**1**), [Cu($\mathbf{L_2H}$)(L_2)(H_2O)](ClO_4) (**2**) and [Cu($\mathbf{L_3H}$)(L_2)](ClO_4) (**3**) with aryl oxime ligands $\mathbf{L_1H}$, $\mathbf{L_2H}$ and $\mathbf{L_3H}$ [$\mathbf{L_1H}$ = 1-(pyridin-2-yl)methanone oxime, $\mathbf{L_2H}$ = 1-(pyridin-2-yl)ethanone oxime and $\mathbf{L_3H}$ = 1-(pyridin-2-yl)propanone oxime] was investigated. All the three ligands have in common a pyridyl group attached to the carbon centre of the oxime moiety and differ in the second substituent attached to the carbon centre. Electrochemical investigation of the catalytic activity of complexes **1**, **2** and **3** shows that the nature of the substituent attached to the carbon centre has an influence on the catalytic pathway and overall catalytic activity of these complexes.

Received 26th June 2024,
Accepted 20th September 2024

DOI: 10.1039/d4dt01852d

rsc.li/dalton

Introduction

With the progress of modern society, the global energy demand is increasing exponentially. Energy sources commonly explored by mankind are fossil fuels, which are non-renewable and depleting at a high rate. Moreover, the wide use of these conventional energy sources leads to environmental pollution, compelling society to move towards green and renewable alternative sources of energy. In this regard, electrocatalytic oxidation of water to yield oxygen and hydrogen is believed to be one of the several alternative pathways to achieve a renewable source of energy.

To date, several homogeneous electrocatalytic water oxidation catalysts with varying degrees of efficiency have been reported. Transition metal complexes have found a good place among these catalysts.[1–4] In this case, the selection of ligands is an important step as ligands play a vital role in the catalytic activity of most of these complexes. Oxidation of water to oxygen requires multiple electron- and proton-transfer reactions. In natural photosynthesis, ligation environments of Mn_4Ca clusters direct the reactivity of the clusters at each step.[5] Metal complexes with a redox-active ligand framework can mimic the activity of oxygen-evolving complexes (OECs) and effectively manage multi-electron transfer reactions by facilitating proton-coupled electron transfer in the course of catalysis.[6–9] Complexes containing oxidation-resistant ligands with highly donating ligation sites are found to be useful in retaining the molecular structure of catalysts under harsh catalytic conditions[10] and stabilising high-valent metal oxo species,[11] a key intermediate postulated in most transition-metal-catalysed water oxidation reactions. Structural features of ligands are also reported to have a profound influence on the reactivity pattern and overall catalytic activity of metal complexes.[12–19]

In this work, we explored the influence of ligand substituents on the electrocatalytic water oxidation activity of transition-metal complexes by comparing the electrocatalytic activity of copper complexes [Cu($\mathbf{L_1H}$)(L_1)](ClO_4) (**1**), [Cu($\mathbf{L_2H}$)(L_2)(OH_2)](ClO_4) (**2**), and [Cu($\mathbf{L_3H}$)(L_2)](ClO_4) (**3**). Among these, **1** and **2** are binary complexes with redox active oxime ligands $\mathbf{L_1H}$ [1-(pyridin-2-yl)methanone oxime] and $\mathbf{L_2H}$ [1-(pyridin-2-yl)ethanone oxime], whereas complex **3** is a ternary complex prepared using ligands $\mathbf{L_2H}$ and $\mathbf{L_3H}$ [1-(pyridin-2-yl)propanone oxime] in equal proportions. All the complexes were characterized by employing different spectroscopic techniques and single-crystal X-ray diffraction. The formation of a ternary complex is evident from the powder XRD pattern of the bulk sample of complex **3**, which closely resembles its simulated pattern (Fig. S15†). Electrocatalytic water oxidation activity of complex **2** in a neutral phosphate buffer has been reported by our group recently.[8] Complex **2** exhibits a remarkably high TOF, nearly equal to 100 s^{-1}.

---

[a] *Department of Chemistry, B. Borooah College, Guwahati 781007, Assam, India. E-mail: apurbakalitabbc@gmail.com*

[b] *Department of Chemistry, IIT Patna, Patna 801103, Bihar, India*

† Electronic supplementary information (ESI) available: Experimental section, FT-IR, UV-visible, NMR spectra, crystallographic data. CCDC 2362016 and 2285154. For ESI and crystallographic data in CIF or other electronic format see DOI: **https://doi.org/10.1039/d4dt01852d**

Results and discussion

The molecular structures of complexes **1**, **2** and **3** were determined by single-crystal X-ray diffraction (Fig. 1). The crystallographic data are given in Table S2.†

To explore the electrochemistry of the copper complexes, their cyclic voltammograms (CV) and differential pulse voltammograms (DPV) were recorded in a 0.1 M neutral sodium phosphate buffer using glassy carbon (GC) as the working electrode, Ag/AgCl as the reference electrode and a platinum wire as the counter electrode in a single-compartment electrochemical cell. The potentials are reported *versus* the normal hydrogen electrode (NHE) by adding 0.197 V to the measured potentials. The cyclic voltammograms (CV) and differential pulse voltammograms (DPV) of complexes **1**, **2** and **3** are depicted in Fig. 2.

The differential pulse voltammograms of complexes **1**, **2** and **3** in the neutral phosphate buffer exhibited five anodic peaks in the potential range from −0.09 V to +1.5 V *vs.* NHE [Fig. 2(b)].

The first anodic peaks of complexes **1**, **2** and **3** appeared at around −0.02, −0.09 and −0.11 V *vs.* NHE, respectively. This electrochemically quasi-reversible peak could be assigned to the Cu^{II}/Cu^{I} couple, which exhibits a pH dependence of ∼0.059 V per pH unit [Fig. S20–S22†], indicating the involvement of one electron and one proton in this step.

The second anodic peaks were found at +0.76, +0.64 and +0.60 V for complexes **1**, **2** and **3**, respectively. Calculations using Laviron equations[20] [Fig. S23–S25†] and the analysis of the Pourbaix diagrams [Fig. S20–S22†] indicate the involvement of one electron and one proton in this step. The UV-visible spectra of the complexes showed distinct changes in the d–d transition region during controlled potential electrolysis (CPE) at the potential of the second anodic peak [Fig. S26†] due to the formation of a Cu(III) species in the complexes (Scheme 1).

The third and fourth anodic peaks of the complexes **1**, **2** and **3** in the potential range of +0.85 to +0.97 V *vs.* NHE were assigned to a ligand-based redox process (Scheme 2) by comparing them with the cyclic voltammograms of analogous Zn^{2+} complexes in the neutral phosphate buffer [Fig. S27–S29†]. The third anodic peaks of all the complexes were found to be pH dependent, and the analysis of the Pourbaix diagrams [Fig. S20–S22†] indicated the involvement of one electron and one proton in this step. The fourth anodic peaks were found to be pH independent for complexes **1** and **2**, whereas, it showed a pH dependency of ∼0.052 V per pH unit in the case of complex **3** (Fig. S22†), leading to the formation of a metal–oxo intermediate. It is believed that the highly electron-donating nature of the ligand substituent in complex **3** allows it to incor-

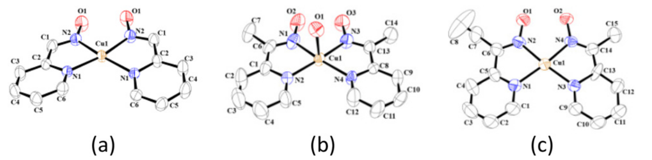

Fig. 1 ORTEP diagrams (50% thermal ellipsoid plot) of (a) complex **1**, (b) complex **2** and (c) complex **3**. Counter anions, hydrogen atoms and solvent molecules are removed for clarity.

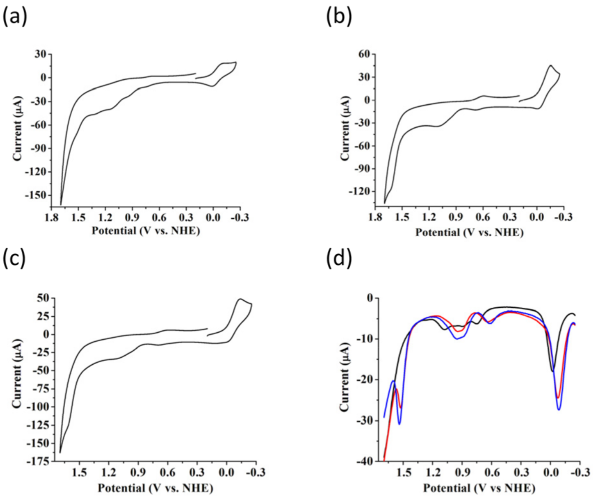

Fig. 2 Cyclic voltammograms of 1 mM solutions of (a) complex **1**, (b) complex **2** and (c) complex **3** in a 0.1 M neutral phosphate buffer at a scan rate of 100 mV s^{-1}. (d) Differential pulse voltammograms (DPV) of complex **1** (black), complex **2** (red) and complex **3** (blue) in a 0.1 M neutral phosphate buffer.

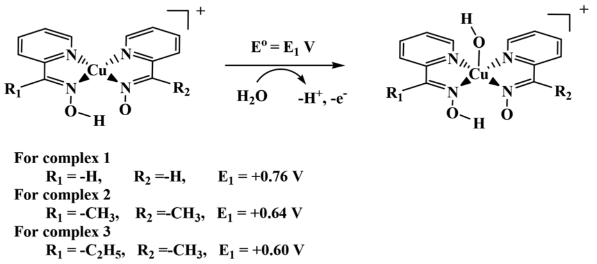

Scheme 1

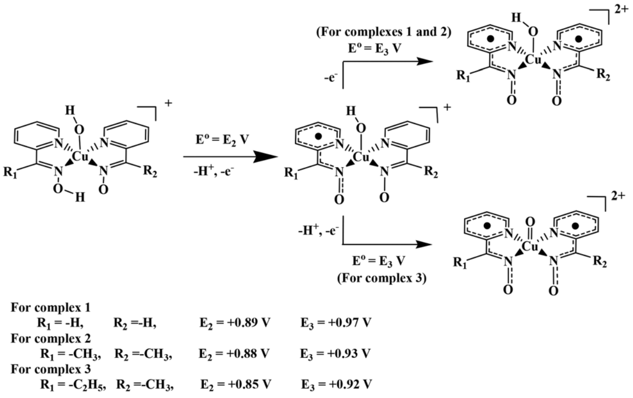

Scheme 2

porate the metal–oxo reactive intermediate in its catalytic cycle, thus overstepping complexes **1** and **2**. To rationalise the possible formation of metal–oxo species, theoretical calculations were carried out using the Gaussian 09 software package.[21] The geometry of the oxo intermediate was optimized using the DFT functional B3LYP and LANL2DZ basis set. Stable geometry was obtained, and vibrational frequency calculations were carried out based on analytical second derivatives at the same level of theory to confirm proper convergence to the local minima. The theoretically optimised structure and the orbital overlap illustration showing the interaction between the metal and the oxo group are shown in Fig. 3.

The high oxidising power that accumulates at this point on the metal complexes drives their reaction with the solvent water molecule and the concomitant formation of the O–O bond. The UV-visible spectra of the complexes during controlled-potential electrolysis at the potential of the respective 4th anodic peaks showed the appearance of a new peak at around 328, 408 and 413 nm for complexes **1**, **2** and **3**, respectively. This peak could be assigned to the formation of the metal–peroxo species[22] (Fig. S49†). Time-dependent DFT (TDDFT) calculations of the optimized structures of the peroxo intermediates obtained from complexes **1**, **2** and **3** were performed (Fig. S59†). The geometries of the peroxo intermediates were optimized using the DFT functional B3LYP and the LANL2DZ basis set. To incorporate the effect of the solvent phase, TDDFT calculations were carried out at the same level of theory in water using the PCM model. TDDFT calculations showed electronic transitions at 358, 385, and 387 nm for complexes **1**, **2** and **3** (Fig. S60, S61 and S62†), respectively, because of the π* → d CT transition, leading to the overlap of the π* orbital of the peroxide ion with a d orbital of the Cu(II) ion. The orbitals associated with the transitions are shown in Fig. S63, S64 and S65,† respectively. The metal–peroxo species formed at this stage of the catalytic cycle of the complexes act differently. For complexes **2** and **3**, it directly oxidises at the respective catalytic potential (E_{cat}) to release the oxygen molecule and regenerate the catalyst (Scheme 3).

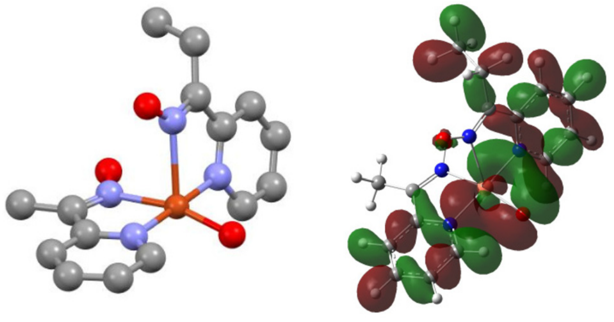

(a) (b)

Fig. 3 (a) DFT-optimised structure of the metal–oxo intermediate [Cu(L$_3^{\bullet}$)(L$_2^{\bullet}$)(O)]$^{2+}$. (b) Boundary surface diagram of the HOMO−12 orbital showing the interaction between the metal center and the oxo group.

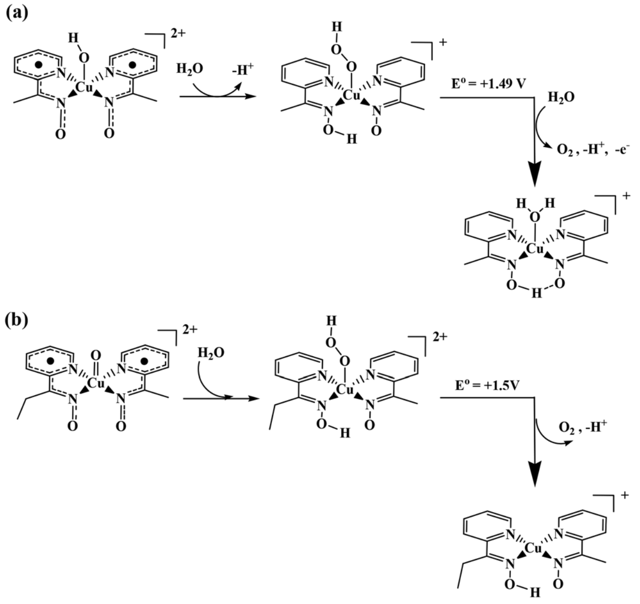

Scheme 3 High-valent metal hydroxo/oxo species generated from (a) complex **2** and (b) complex **3** react with water to generate the hydroperoxo complexes that further oxidise to release the oxygen molecule.

The peroxo species generated from complex **1** concomitantly react with another ground state complex to form a peroxo bridge dimer (Cu^{III}–O–O–Cu^{II}), Scheme 4 which exhibit one electron oxidation peak at +1.08 V vs. NHE to form Cu^{III}-O-O-Cu^{III} species (Scheme 4).This species is further oxidised at 1.51 V *vs.* NHE, releasing an oxygen molecule and regenerating the catalyst.

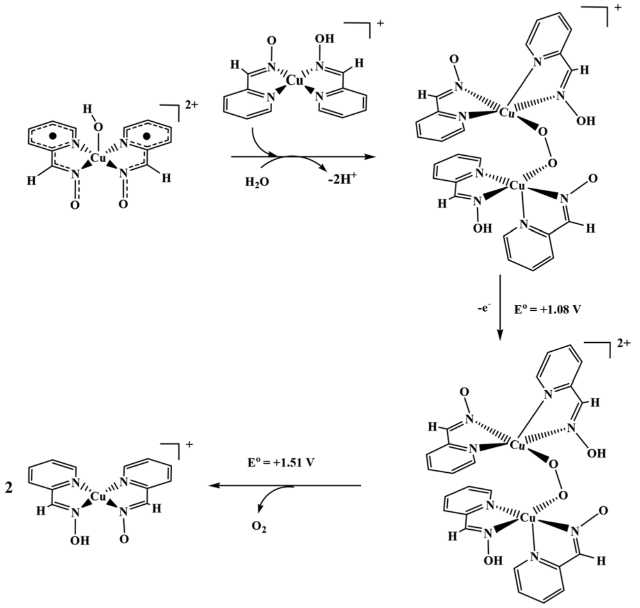

Scheme 4 Plausible reaction pathway of the formation of the peroxo bridge dimer from the high-valent metal–hydroxo species generated from complex **1** and its concomitant oxidation, leading to the release of the oxygen molecule and regeneration of the catalyst.

The formation of the dimeric species was evident from the concentration variation study at the peak current of complex **1** (Fig. S31†). It was found that the peak current varied linearly with the concentration of the complex till the fourth anodic peak, but for the fifth anodic peak, it varied linearly with the square of the concentration of complex **1** (Fig. S32†).

To obtain kinetic information of the catalytic process, a foot-of-the-wave analysis was carried out according to the methodology described by Savéant *et al.*[23] Under catalytic conditions, eqn (1) is operative for oxidation involving four electrons.

$$i_{\mathrm{cat}}/i_{\mathrm{d}} = \left[2.24n(RTk_{\mathrm{obs}}/F\nu)^{1/2}\right]/\left[1+\exp\left\{\left(E^{\circ}_{\mathrm{cat}}-E\right)F/RT\right\}\right] \tag{1}$$

where E°_{cat} is the standard potential of the catalysis-initiating redox couple, i_{cat} is the current intensity in the presence of the substrate, i_{d} is the current intensity in the absence of the substrate, n (= 4) is the number of electrons involved in the catalytic cycle, F is the Faraday constant, ν is the scan rate, k_{obs} is defined as $k_{\mathrm{cat}} \times C^{\circ}_{\mathrm{A}}$ (C°_{A} is the concentration of substrate; 55.56 M for water), and R is gas constant (8.314 J mol^{-1} K^{-1}). The background-corrected CVs of the complexes at different scan rates are shown in Fig. 4.

Then, k_{obs} were extracted from the plots of $i_{\mathrm{cat}}/i_{\mathrm{d}}$ *versus* $1/\left\{1+\exp\left[(F/RT)\left(E^{\circ}_{\mathrm{cat}}-E\right)\right]\right\}$, as shown in (Fig. S35, S37 and S39) in the ESI.† The largest slopes at the very beginning of the catalytic process showed the values of $k_{\mathrm{obs}} \sim 32$ s^{-1}, ~100 s^{-1} and ~248 s^{-1} for complexes **1**, **2** and **3**, respectively. Catalytic activity in terms of TOF was found to increase with the electron-donating ability of the substituents attached to the carbon center of the oxime moiety. In Table 1, the TOF values and the reaction conditions of some recently reported copper-based water oxidation catalysts are summarized.

The onset potential for water oxidation was located close to 1.51, 1.49 and 1.52 V *vs.* NHE for complexes **1**, **2** and **3**, respectively (Fig. S34†). The overpotentials of the 1 mM solutions of complexes **1**, **2** and **3** to attain a current density of 1 mA cm^{-2} were determined to be ~693 mV, ~675 mV, and ~703 mV, respectively.

Oxygen evolution was investigated through controlled-potential electrolysis (CPE) at 1.51, 1.49 and 1.52 V *vs.* NHE for complexes **1**, **2** and **3**, respectively, using a large-surface-area ITO working electrode (4 cm^2) in a gas-tight cell (Fig. S44†). The oxygen formed in the solution was measured using a calibrated Ocean Optics FOXY probe. Faradaic efficiency values close to 90%, 94% and 95% were estimated based on the long-term electrolysis study of complexes **1**, **2** and **3**, respectively (Fig. S45, S46 and S47†). The CV and UV-visible spectra of the complexes recorded before and after the bulk electrolysis experiment were almost identical (Fig. S48 and S49†). The total charge passed after 1 h of electrolysis under the same conditions varied linearly with the initial concentration of the complexes [Fig. 5 and S41–S43†] with no evidence of an induction period at the early stage of electrolysis, providing evidence for homogeneous water oxidation catalysis. The CVs recorded with the ITO working electrode before and after each electrolysis experiment in the absence of the catalyst were essentially identical (Fig. S50–S52†). The FE-SEM and EDX data of the fresh and used ITO working electrodes showed no evidence of deposition of the electroactive species on the working electrode surface during the long-term electrolysis experiment (Fig. S53–S58†) of the complexes. The lack of evidence for a new electroactive species adsorbed on the working electrode or

Table 1 Kinetic data of complexes **1**, **2**, **3** and some related copper based water oxidation catalysts

Catalyst structure	Ligand substituent	pH	TOF (s^{-1})	Ref.
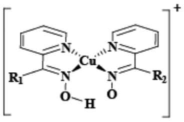	$R_1 = R_2 = H$	7.0	32	T.W.
	$R_1 = R_2 = Me$	7.0	100	T.W.
	$R_1 = Me, R_2 = Et$	7.0	248	T.W.
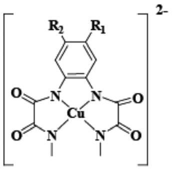	$R_1 = R_2 = H$	11.5	3.56	9
	$R_1 = R_2 = Me$	11.5	3.58	9
	$R_1 = H, R_2 = OMe$	11.5	0.43	9
	$R_1 = R_2 = OMe$	11.5	0.16	9
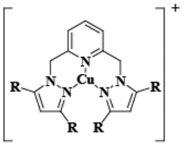	R = H	6.5	0.33	17
	R = Me	6.5	9.77	17
	R-*t*-Bu	6.5	0.30	17
	R = Ph	6.5	1.47	17
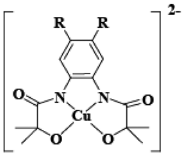	R = H	9.2	54	18
	R = Me	9.2	—	18

T.W. stands for this work.

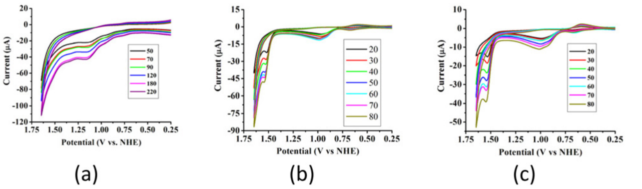

Fig. 4 Background-corrected CVs of 0.5 mM solutions of (a) complex **1**, (b) complex **2** and (c) complex **3** in a 0.1 M neutral phosphate buffer at different scan rates.

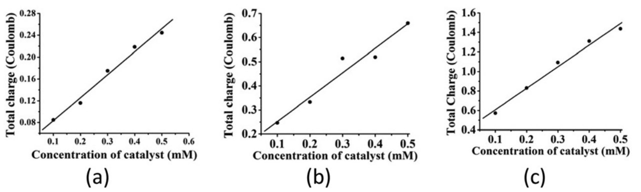

Fig. 5 Plots of total charge *vs.* concentration after 1 h of electrolysis: (a) complex **1**, (b) complex **2** and (c) complex **3**.

present in the electrolyte mixture collectively indicates homogeneous catalysis. All three complexes also showed activity towards chemically driven water oxidation with CAN as the primary chemical oxidant (Fig. S67 and Table S7†).

Conclusions

In conclusion, complexes **1**, **2** and **3** with similar first coordination environments behave as stable homogeneous electrocatalysts for water oxidation in a neutral pH medium. In all these complexes, the copper(II) metal ion is coordinated with the oxime ligand, but they have different alkyl substituents attached to the oxime carbon. Electrochemical investigation reveals that complexes **1**, **2** and **3** behave differently on the working electrode during the electrocatalytic process. The ternary complex **3** with ethyl and methyl substituents attached to the oxime ligands stabilises and incorporates the highly oxidising metal–oxo intermediate at a relatively lower electrode potential, which in turn catalyses the formation of the O–O bond with a high TOF (~248 s^{-1}). Complex **1** with an aldoxime ligand prefers a bimolecular pathway to catalyse the water oxidation reaction with a relatively low TOF (~32 s^{-1}). The homoleptic complex **2** with a methyl substituent attached to the oxime ligands exhibits a TOF of ~100 s^{-1}, which is lower than that of complex **3** but greater than that of complex **1**. This difference in catalytic behaviour of the complexes is believed to originate from differences in the electron-donating ability and steric effect of the substituents attached to the carbon center of the oxime moiety.

Experimental section

Materials and methods

All reagents and solvents were purchased from commercial sources and were of reagent grade. The UV-visible spectra were recorded on a Cary-60 UV-visible spectrophotometer. The FT-IR spectra were recorded on a Cary 630 spectrophotometer with the samples prepared as KBr pellets. Elemental analyses were carried out on a Thermo Scientific Flashsmart Analyzer. Electrochemical measurements were recorded using a CHI 7035E bipotentiostat. The single-crystal data were collected on a BRUKER AXS (D8 Quest System) X-ray diffractometer equipped with a PHOTON 100 CMOS detector at 293(2) K. The X-ray generator was operated at 50 kV and 30 mA using Mo Kα (λ = 0.71073 Å) radiation.

Synthesis of ligand L_1H

To a solution of pyridine-2-carboxyaldehyde (2 g, 18.69 mmol) in methanol, hydroxylamine hydrochloride (3.24 g, 46.62 mmol) and sodium carbonate (4.9 g, 46.22 mmol) were added with constant stirring. The reaction mixture was refluxed for 1.5 h at 60 °C. After the completion of the reaction, the reaction mixture turned light pink. The reaction mixture was then filtered, and the filtrate was used for crystallization. The white crystals obtained were dried and weighed. Yield: 2.30 g (~82%). Ligand **L_1H** was characterized by FT-IR, ^{1}H-NMR and ^{13}C-NMR spectroscopy. FT-IR (KBr pellet): 3483, 3016, 1594, 1512, 1437, 1329, 1000, 792, 735, and 665 cm^{-1}; ^{1}H-NMR (400 MHz, $CDCl_3$): δ_{ppm}, 8.62, 7.82, 7.75, 7.70, 7.27, and 4.45. ^{13}C-NMR (100 MHz, CD_3Cl_3): δ_{ppm}, 151.76, 148.97, 137.23, 124.10, 121.27, and 48.99. Mass: $(m + H^+)/z$: calcd 123.05; found, 123.91.

Synthesis of ligand L_2H

To a solution of acetylpyridine (1 g, 8.2 mmol) in methanol, hydroxylamine hydrochloride (0.63 g, 9.0 mmol) and sodium carbonate (1.3 g, 1.22 mmol) were added with constant stirring. The reaction mixture was refluxed for 1.5 h at 60 °C. After the completion of the reaction, the reaction mixture turned light pink. The reaction mixture was then filtered, and the filtrate was used for crystallization. The white crystals obtained were dried and weighed. Yield: 0.930 g (~84%). Ligand **L_1H** was characterized by FT-IR, ^{1}H-NMR and ^{13}C-NMR spectroscopy. FT-IR (KBr pellet): 3178, 2846, 1594, 1490, 1438, 1000, 933, 829, 785, and 681 cm^{-1}; ^{1}H-NMR (400 MHz, CD_3COCD_3): δ_{ppm}, 10.58, 8.55, 7.87, 7.29, 2.90, and 2.27. ^{13}C-NMR (100 MHz, CD_3COCD_3): δ_{ppm}, 154.97, 148.78, 136.06, 123.41, 119.87, 87.22, and 9.36.

Synthesis of ligand L_3H

To a stirred suspension of finely pulverized KOH (5.6 g, 0.1 mmol) in toluene (30 mL), 18-crown-6 (0.26 g, 1 mmol) and 2-acetylpyridine (1.21 g, 10 mmol) were added. MeI (11.4 g, 80 mmol) was added dropwise to the orange reaction mixture, which immediately caused an exothermic reaction. The mixture was stirred at room temperature. After 19 h, the mixture turned pale yellow. After filtration, the solvent was evaporated at reduced pressure, and the residue was distilled in a vacuum to give 1.0 g (67%) of ketone (1-(pyridin-2-yl)propan-1-one). To a solution of 1-(pyridin-2-yl)propan-1-one (1.5 g, 10 mmol) dissolved in methanol, hydroxylamine hydrochloride (1.38 g, 19.85 mmol) and sodium carbonate (2.12 g, 20 mmol) were added with constant stirring. The reaction mixture was refluxed for 1.5 h at 60 °C. After the completion of the reaction, the reaction mixture turned light pink. The reaction mixture was then filtered, and the filtrate was used for crystallization. The white crystals obtained were dried and weighed. Yield: 1.45 g (~87%). Ligand **L_2H** was characterized by FT-IR, ^{1}H-NMR and ^{13}C-NMR spectroscopy. FT-IR (KBr pellet): 3170, 2854, 1594, 1487, 1006, 935, and 800 cm^{-1}. ^{1}H-NMR (400 MHz, $CDCl_3$): δ_{ppm}, 8.50, 7.84, 7.73, 7.30, 2.90, 2.25, 1.25, and 1.07. ^{13}C-NMR (100 MHz, CD_3Cl_3): δ_{ppm}, 9.76, 19.22, 120.93, 123.30, 138.60, 148.20, 154.78, and 162.31.

Synthesis of complex 1, $[Cu(L_1H)(L_1)](ClO_4)$

Copper(II) perchlorate hexahydrate with the formula $[Cu(H_2O)_6](ClO_4)_2$ (0.303 g, 0.818 mmol) was dissolved in 25 mL methanol, and to this blue solution, ligand **L_1H** (0.2 g, 1.64 mmol) was added dropwise. The color of the solution changed from blue to green. The resulting mixture was stirred for 1 h. Then, the volume of the solution was reduced to

~10 mL. It was then kept for crystallization at room temperature, which resulted in green crystalline compounds. Yield: 0.52 g (~75%). UV-visible (methanol): $\lambda_{\max}$, 650 nm (ε = 227 M^{-1} cm^{-1}). FT-IR (KBr pellet): 3445, 1607, 1563, 1474, 1341, 1120, 905, and 780 cm^{-1}. Molar conductance: 182 S cm^2 mol^{-1} (water), 139 S cm^2 mol^{-1} (acetonitrile). The observed magnetic moment was found to be 1.83μ_B.

Synthesis of complex 2, $[Cu(L_2H)(L_2)(H_2O)](ClO_4)$[24]

Copper(II) perchlorate hexahydrate $[Cu(H_2O)_6](ClO_4)_2$ (0.68 g, 1.8 mmol) was dissolved in 25 mL methanol, and to this blue solution, ligand **L_2H** (0.5 g, 3.6 mmol) was added dropwise. The color of the solution changed from blue to dark green. The resulting mixture was stirred for 1 h. Then, the volume of the solution was reduced to ~10 mL. It was then kept for crystallization at room temperature, which resulted in green crystalline compounds. Yield: 0.68 g (~79%). UV-visible (methanol): $\lambda_{\max}$, 580 nm (ε = 138 M^{-1} cm^{-1}). FT-IR (KBr pellet): 3505, 1607, 1472, 1139, 1087, 779, and 616 cm^{-1}. Molar conductance: 117 S cm^2 mol^{-1}. The observed magnetic moment was found to be 1.7μ_B.

Synthesis of complex 3, $[Cu(L_3H)(L_2)](ClO_4)$

To a methanolic solution of **L_2H** (0.18 g, 1.32 mmol) and **L_3H** (0.2 g, 1.33 mmol) in a 50 mL round-bottom flask equipped with a magnetic stirring bar, copper(II) perchlorate hexahydrate, $[Cu(H_2O)_6](ClO_4)_2$ (0.49 g, 1.32 mmol) dissolved in methanol, was added drop-wise. The colour of the solution changes to dark green. The resulting mixture was stirred for 1 h. Then, the volume of the solution was reduced to ~10 mL. It was then kept for crystallization at room temperature, which resulted in green crystalline compounds. Yield: 0.25 g (~82%). Elemental analyses: calcd for $C_{15}H_{17}N_4O_6ClCu$: C, 40.19; H, 3.82; N, 12.50. Found (%): C, 40.24; H, 3.83; N, 12.46. UV-visible (methanol): $\lambda_{\max}$, 570 nm (ε = 223 M^{-1} cm^{-1}). FT-IR (KBr pellet): 3458, 1616, 1481, 1093, and 783 cm^{-1}. Molar conductance: 154 S cm^2 mol^{-1}. The observed magnetic moment was found to be 1.78μ_B.

Data availability

The data supporting this article have been included as part of the ESI.† Crystallographic data for the structures reported in this article have been deposited with the Cambridge Crystallographic Data Centre (CCDC) under deposition numbers 2362016 and 2285154.†

Conflicts of interest

There are no conflicts to declare.

Acknowledgements

A. K. would like to thank the Department of Science and Technology (SERB), India for financial support (award no. YSS/2015/000878). The authors are also grateful to Department of Chemistry, IISER Tirupati and SAIF IIT Patna for single crystal XRD data. H. K. gratefully acknowledges UGC for providing research fellowships (candidate ID: NFO-2018-19-OBC-ASS-71019).

Notes and references

1 H. Lee, X. Wu and L. Sun, Copper based homogeneous and heterogeneous catalysts for electrochemical water oxidation, *Nanoscale*, 2020, **12**, 4187–4218.

2 M. K. Coggins, M. T. Zhang, A. K. Vannucci, C. J. Dares and T. J. Meyer, Electrocatalytic water oxidation by a monomeric amidate ligated Fe(III)–aqua complex, *J. Am. Chem. Soc.*, 2014, **136**, 5531–5534.

3 N. McMillion, A. W. Wilson, M. K. Goetz, M. Chang, C. Lin, W. Feng, C. McCroryand and J. S. Anderson, Imidazole for pyridine substitution leads to enhanced activity under milder conditions in cobalt water oxidation electrocatalysis, *Inorg. Chem.*, 2019, **58**(2), 1391–1397.

4 M. Aligholivand, Z. Shaghaghi, R. Bikas and A. Kozakiewicz, Electrocatalytic water oxidation by a Ni(II) salophen type complex, *RSC Adv.*, 2019, **9**, 40424–40436.

5 J. Yanoand and V. Yachandra, Mn_4Ca cluster in photosynthesis: Where and how water is oxidized to dioxygen, *Chem. Rev.*, 2014, **114**, 4175–4205.

6 D. Wang and C. Bruner, Catalytic water oxidation by a bioinspired nickel complex with a redox-active ligand, *Inorg. Chem.*, 2017, **22**, 13638–13641.

7 J. S. Pap, Ł. Szyrwiel, D. Sranko, Z. Kerner, B. Setner, Z. Szewczuk and W. Malinka, Electrocatalytic water oxidation by Cu(II) complexes with branched peptides, *Chem. Commun.*, 2015, **51**, 6322–6324.

8 H. Kuilya, N. Alam, D. Sarma, D. Choudhury and A. Kalita, Ligand assisted electrocatalytic water oxidation by a copper (II) complex in neutral phosphate buffer, *Chem. Commun.*, 2019, **55**, 5483–5486.

9 P. G. Barros, I. F. Ardoiz, S. Drouet, J. B. Buchholz, F. Maseras and A. Llobet, Redox Non-Innocent Ligand Controls Water Oxidation Overpotential in a New Family of Mononuclear Cu-Based Efficient Catalysts, *J. Am. Chem. Soc.*, 2015, **21**, 6758–6761.

10 K. J. Fisher, K. L. Materna, B. Q. Mercado, R. H. Crabtree and G. W. Brudvig, Electrocatalytic Water Oxidation by a Copper(II) Complex of an Oxidation-Resistant Ligand, *ACS Catal.*, 2017, **7**, 3384–3387.

11 D. Das, S. Pattanayak, K. K. Singh, B. Garaib and S. S. Gupta, Electrocatalytic water oxidation by a molecular cobalt complex through a high valent cobalt oxo intermediate, *Chem. Commun.*, 2016, **52**, 11787–11790.

12 J. Shen, X. Zhang, M. Cheng, J. Jiang and M. Wang, Electrochemical Water Oxidation Catalyzed by N_4-Coordinate Copper Complexes with Different Backbones Insight into the Structure-Activity Relationship of Copper Catalysts, *ChemCatChem*, 2020, **12**, 1302–1306.

13 J. W. Wang, C. Hou, H. H. Huang, W. J. Liu, Z. F. Ke and T. B. Lu, Further insight into the electrocatalytic water oxi-

dation by macrocyclic nickel(II) complexes-the influence of steric effect on catalytic activity, *Catal. Sci. Technol.*, 2017, **7**, 5585–5593.

14 M. Zhang, M. T. Zhang, C. Hou, Z. F. Ke and T. B. Lu, Homogeneous Electrocatalytic Water Oxidation at neutral pH by a robust macrocyclic Nickel(II) complex, *Angew. Chem., Int. Ed.*, 2014, **53**, 13042–13048.

15 J. Shen, M. Wang, J. Gao, H. Han, H. Liu and L. Sun, Improvement of Electrochemical Water Oxidation by Fine-Tuning the Structure of Tetradentate N_4 Ligands of Molecular Copper Catalysts, *ChemSusChem*, 2017, **10**, 4581–4588.

16 D. L. Gerlach, S. Bhagan, A. A. Cruce, D. B. Burks, I. Nieto, H. T. Truong, S. P. Kelley, C. J. Herbst-Gervasoni, K. L. Jernigan, M. K. Bowman, S. Pan, M. Zeller and E. T. Papish, Studies of the Pathways Open to Copper Water Oxidation Catalysts Containing Proximal Hydroxy Groups During Basic Electrocatalysis, *Inorg. Chem.*, 2014, **53**, 12689–12698.

17 T. Makhado, B. Das, R. J. Kriek, H. C. M. Vosloo a and A. J. Swarts, Chemical and electrochemical water oxidation mediated by bis(pyrazol-1-ylmethyl)pyridine-ligated Cu(I) complexes, *Sustainable Energy Fuels*, 2021, **5**, 2771–2780.

18 M. Bera, K. Keshari, A. Bhardwaj, G. Gupta, B. Mondal and S. Paria, Electrocatalytic water oxidation activity of molecular copper complexes: Effect of redox-active ligands, *Inorg. Chem.*, 2022, **61**, 3152–3165.

19 S. Chattopadhyay, A. Ghatak, Y. Ro, R. Guillot, Z. Halime, A. Aukauloo and A. Dey, Ligand radical mediated water oxidation by a family of copper o-phenylenebis-oxamidate complexes, *Inorg. Chem.*, 2021, **60**, 9442–9455.

20 E. Laviron, General Expression of the linear potential sweep voltammogram in the case of diffusionless electrochemical systems, *J. Electroanal. Chem.*, 1979, **101**, 19–28.

21 M. J. Frisch, G. W. Trucks, H. B. Schlegel, G. E. Scuseria, M. A. Robb, J. R. Cheeseman, G. Scalmani, V. Barone, B. Mennucci, G. A. Petersson, H. Nakatsuji, M. Caricato, X. Li, H. P. Hratchian, A. F. Izmaylov, J. Bloino, G. Zheng, J. L. Sonnenberg, M. Hada, M. Ehara, K. Toyota, R. Fukuda, J. Hasegawa, M. Ishida, T. Nakajima, Y. Honda, O. Kitao, H. Nakai, T. Vreven, J. A. Montgomery, J. E. Peralta, F. Ogliaro, M. Bearpark, J. J. Heyd, E. Brothers, K. N. Kudin, V. N. Staroverov, T. Keith, R. Kobayashi, J. Normand, K. Raghavachari, A. Rendell, J. C. Burant, S. S. Iyengar, J. Tomasi, M. Cossi, N. Rega, J. M. Millam, M. Klene, J. E. Knox, J. B. Cross, V. Bakken, C. Adamo, J. Jaramillo, R. Gomperts, R. E. Stratmann, O. Yazyev, A. J. Austin, R. Cammi, C. Pomelli, J. W. Ochterski, R. L. Martin, K. Morokuma, V. G. Zakrzewski, G. A. Voth, P. Salvador, J. J. Dannenberg, S. Dapprich, A. D. Daniels, O. Farkas, J. B. Foresman, J. V. Ortiz, J. Cioslowski and D. J. Fox, *Gaussian 09, Revision A.1*, Gaussian, Inc., Wallingford, CT, 2009.

22 L. M. Mirica, X. Ottenwaelder and T. D. P. Stack, *Chem. Rev.*, 2004, **104**, 1013–1045.

23 C. Costentin, S. Drouet, M. Robert and J. M. Savéant, Turnover Numbers, Turnover Frequencies, and Overpotential in Molecular Catalysis of Electrochemical Reactions. Cyclic Voltammetry and Preparative-Scale Electrolysis, *J. Am. Chem. Soc.*, 2012, **134**, 11235–11242.

24 Complex **2** was reported earlier from our research group (article: DOI: **10.1039/C9CC00971J**).